LUND UNIVERSITY

THESIS SUBMITTED FOR DEGREE OF BACHELOR OF SCIENCE

PROJECT DURATION: 15 HP

Real-time Entanglement of Auger and XPS Electrons: a preliminary investigation

Author:

Philip JOHANSSON

Supervisor:

Claudio VERDOZZI

Co-Supervisors:

Mathieu GISSELBRECHT

Emil VIÑAS BOSTRÖM

DEPARTMENT OF PHYSICS

DIVISION OF MATHEMATICAL PHYSICS

Abstract

In this work, we employ a semi-classical approach to light matter interaction to describe and characterize spin configurations resulting from quantum correlations between electrons created by a photoemission event and by the following Auger decay. The system studied consists of three atomic levels and two continua. Initially, an external classical light field, in the form of a narrow Gaussian packet, perturbs the system, and transfers the density of charge, corresponding to one electron (the photoelectron), from the core level to the continuum. The Auger decay then occurs, whereby an electron from either of the valence levels decay to the core while, at the same time, another electron (the Auger electron) is emitted to the continuum. The description of the system is performed in the time domain, by time-evolving the many-particle wave function. Tracking the density of charge in the atomic levels and the continuum levels allows for a description of the dynamics of photoemission and Auger decay. Calculating the concurrence, as measure of entanglement, between the photoelectron and the Auger electron, gives insight about the correlation between their spins.

We consider two scenarios; altering the relative strengths of the matrix elements responsible for anti-parallel and parallel spin configuration while keeping the interaction between the photoelectron and the Auger electron fixed, and secondly varying the interaction while keeping all the matrix elements fixed. The effect of increasing the strength of the parallel-spin configuration can be seen in the concurrence decreasing, diminishing the correlation between the spin of the photo- and the Auger electron. Furthermore, we find that the interactions between the electrons in the continuum strongly affect the modality of entanglement.

While giving a rather simplistic description of a realistic atomic system, our results support the scope of the model to give valuable conceptual insight, into novel qualitative aspects of the temporal dynamics of the Auger decay.

Acknowledgments

Firstly, I would like to express my gratitude to my supervisors Claudio Verdozzi, Mathieu Gisselbrecht and Emil Viñas Boström for taking time out of their days to help me and guide me through this project. I especially want to thank Claudio for introducing me to this topic and field. He showed me that I had a lot to learn, and was there to help me learn all the methods and theory required for this project. Emil has been a great source of feedback and assistance when it came to theory and coding, which is central to the project and I am thus very grateful for this. Mathieu has given me insight into the more applied side of the work, how Auger decay can be used to study various things, as well as he has helped me understand the relation between parameters in the project. This has led me to understand the outcomes on a more physical basis.

Secondly, I would like to thank Andrea Idini, Jakob Bengtsson and Eric Ceccarelli; Andrea and Jakob for giving me access to the cluster at the mathematical physics division, as well as helping me sort out problems with compilation; Eric for teaching me how to use the cluster.

Abbreviations

PE : photoelectron
AE : Auger electron

Contents

Chapter 1

Introduction and Motivation

Photo emission is a fundamental process in quantum mechanics, and was in part responsible for the birth of the subject. The 19th century provided evidence of a seemingly odd behavior of bound electrons being excited by light [1]. According to classical Maxwell theory, the energy of an electromagnetic field is proportional to the square of the field strength [2], hence if the energy of the field exciting a bound electron exceeds the binding energy of the electron one would expect that, no matter the color of the light, raising the intensity to some threshold intensity would be sufficient to ionize electrons. This turned out not to be the case as Philipp Lenard found [1] that it instead and in fact depended on the color (an anachronism for "frequency").

At the turn of the century Max Planck postulated, as a mathematical trick, that light was not a field in the Maxwell sense, but quanta of energy[3]. This led to the solution of not one, but two paradoxes of that time; the ultraviolet catastrophe and frequency depending light in contrast with Maxwell. Albert Einstein took this idea of quanta of energy, photons, and formalized a theory of the photoelectric effect[4].

With this new theory of light and with quantum mechanics on the rise it became possible to study the inner workings of atoms more closely and accurately. One such investigation was performed, in parallel, by Lise Meitner[5] and Pierre Auger[6], Auger credited with the name although Meitner discovered it first. They found that if a core electron is ionized from an atom, a Coulombic readjustment of electrons can occur where one electron fills the hole which leads to the emission of another.

The study of the kinetic energy of Auger electrons is referred to as Auger electron spectroscopy and, together with photoemission, Auger electron spectroscopy provides the tools to study core hole dynamics in atoms and core hole localization in molecules [7]. Furthermore, as the progress in ultra short laser pulses is advancing, systems that can undergo Auger decay are suitable for studies of ultrafast atomic processes as well as pioneering research about the Quantum Zeno Effect, QZE[8].

In the case of materials, the photoelectric and Auger effects have been used extensively since the middle of the 20th century, when technology to resolve electron energies became good enough,

to perform chemical analysis of complex compounds, e.g. solid surfaces, adsorbates and alloys by analyzing the photoelectrons and especially the Auger spectra (the latter containing energies which are fingerprint of the specific transition occurred, and thus of the type of atomic element involved [9]).

There is however something else that these two effects can be used to study, that is more applicable and highly relevant for many current research ares in physics: entanglement. One talks about entanglement when the state of a system cannot be decomposed into its subsystems, i.e. when the state vector cannot be factorised into a tensor-product of states of each subsystem. Entanglement can lead to non-classical correlations and these correlations can be used to perform ultra fast probings of core hole localization[7], and is also a basic resource for realizing quantum computers[10]. It is hence of use, and possible, to study entanglement, and systems that bring about entangled pairs of electrons.

For this reason, this thesis is designed to perform a theoretical investigation into an atomic model system that undergoes photoemission followed by an Auger decay. We study the real time dynamics of these processes and calculate the entanglement between the final state photoelectron and Auger electron using concurrence, which is a widely used indicator of entanglement.

It is worthwhile at this point to the emphasize the high degree of novelty of our study. Time-dependent studies of the Auger decay are still rare, and often require a number of approximations to be made in the treatment. One such approximation (and a rather common one) is to leave out an explicit description of the photoelectron in the continuum, under the assumption that this electron is very fast (due to the high frequency of the light) and interacts negligibly with the system left behind. While this considerably simplifies the description, it also automatically excludes the possibility to study the interaction between the photo- and the Auger electron, and a characterization of entanglement becomes not possible. With the method introduced here, this relationship between the two electrons, albeit in an oversimplified model system and with an approximation in the treatment, is accessible, and its dynamical emergence/establishment can be characterized in the time domain.

Chapter 2

Atoms and Electron Spectroscopy

We provide here a short conceptual background to Auger and photoelectron spectroscopies.

2.1   Photoelectric effect and photoemission spectroscopy

The Photoelectric effect describes the process where a highly energetic photon is absorbed by an atom, leading to the emission of an electron. In Einstein's work on the photoelectric effect, it is proposed that the energy of a photon is proportional to the frequency of the light[4]:

$$E_\gamma = h\nu. \tag{2.1.1}$$

When the energy of the photon exceeds the binding energy of an electron in an atom, also referred to as the ionization potential I, the electron will be released into a continuum of states with a kinetic energy corresponding to the difference between the photon energy and the ionization potential. The maximum kinetic energy of an photoemitted electron is thus:

$$E_k = h\nu - I \tag{2.1.2}$$

Hence, by exposing a material to monochromatic light of frequency ν and measuring the energy of the electrons, one can determine the binding energies of electrons, from equation 2.1.2, and thus study the electronic structure of matter. The study of the kinetic energy of the electron as a result of photoemission is referred to as electron spectroscopy and since the middle of the 19th, electron spectroscopy has been extensively employed to investigate atomic and molecular orbitals and in general electronic properties of condensed matter [11].

In order to understand the rate of transition from an initial state, $|i\rangle$, to a final state, $|f\rangle$, we turn to a semi-classical approach where the interacting electromagnetic field is taken to be classical. In this approach the light field continuously transfers the density of charge, i.e. the population, of an electron to the continuum, as opposed to quantized light that promptly creates a hole, a quasi-particle corresponding to the lack of an electron, in the initial state.

Under the assumption that the intensity of the light field is weak enough, one can treat the field as a perturbation to the system and thus calculate the transition probability, $\mathcal{P}_{i \to f}$, for a transition between the initial state, $|i\rangle$, to the final state, $|f\rangle$, within a perturbation theory. In the Göbbert Mayer gauge, and dipole approximation, the interaction Hamiltonian, in the second quantization formalism[12], is given by[13]:

$$H_I(t) = -\boldsymbol{d} \cdot \boldsymbol{E} \cos(\omega t)(a_f^\dagger a_i + \text{H.c.}) = M_{if} \cos(\omega t)(a_f^\dagger a_i + \text{H.c.}) \tag{2.1.3}$$

where $\omega = \nu/2\pi$, ν is taken to be close to the resonance frequency of the transition and $M_{if} = -\langle i| \boldsymbol{d} \cdot \boldsymbol{E} |f\rangle$ represents the dipole matrix element between the initial and final state. In more general instances where the initial state is coupled to a continuum of levels, the interaction Hamiltonian couples the initial state to all the continuum levels in the same manner as in equation 2.1.4:

$$H_{ph}(t) = \sum_q M_q \cos(\omega t)(a_{f_q}^\dagger a_i + \text{H.c.}) \tag{2.1.4}$$

where the f_q represent a continuum level of energy ϵ_q and the set $\{|i\rangle,\ |f_q\rangle\,;\ q = 1, 2, ...N\}$ form a complete set of states for the Hilbert space of dimension $N + 1$. Finally, the transition probability between two configurations of states $|i\rangle$ and $|f_q\rangle$, with the distinction that now $|f_q\rangle$ refers to the states with an electron in the continuum with energy ϵ_q, is given by:

$$\mathcal{P}_{i \to f}(\omega) = \sum_q \frac{2\pi}{\hbar} |M_q|^2 \rho(E_i - E_{f_q} - \hbar\omega) \tag{2.1.5}$$

2.2 The Auger Effect and Auger Electron Spectroscopy

When the energy of the light used to ionize an atom is high enough, a deeply bound electron (a core electron) may be emitted, resulting in the atom being left out of equilibrium with a hole in the core level. A valence level electron can then relax to the core, transferring, nonradiatively, its excess energy to another electron in the atom. If the energy provided to the second electron is greater than the ionization potential of the ion, that electron is emitted from the atom with energy:

$$\epsilon_A = \epsilon_g - \epsilon_{v_i v_j}, \tag{2.2.1}$$

where ϵ_g is the energy of the ground state and $\epsilon_{v_i v_j}$ represents the energy of the state with vacancies in valence levels i and j, including any inter-/intrashell interactions/relaxations. This expression can be made more explicit looking separately at different contributions, and considering explicitly the core/Auger channels involved[14, 15]. In a more rigorous description, the Auger decay corresponds to a transition (mediated by the Coulomb interaction) between an initial two-hole state (one in the core and one in the continuum) to a final state with two vacancies in the higher energy levels of the atom.

The Auger process is a common occurrence in lighter elements, while for heavier elements a dipole transition dominates, where a valence electron relaxes to the hole emitting its excess energy as light[11].

The dynamics of photoemission followed by Auger decay can be treated in a one-step or two-step approach. In the two-step approach, the photoemission is not affected by the Auger decay. Firstly, photoemission is treated, with an interaction Hamiltonian as in equation 2.1.4. Once the density of charge in the continuum corresponds to that of one electron, a second step is considered using the final state of the photoemission as initial state for the Auger decay. The second part of the process is induced by the Auger interaction Hamiltonian:

$$H_A = \sum_k M_k(a_c^\dagger a_k^\dagger a_i a_j + \text{H.c.}),$$
(2.2.2)

where M_k is the matrix element of the Coulomb interaction between the initial and final state, and as before, $|f_k\rangle$ represents a state with an electron in the continuum with energy ϵ_k, (a complete discussion of the atomic Auger matrix elements can be found in [16]). Equation 2.2.2 then describes the process of an electron relaxing from a valence level to the core while an electron simultaneously is emitted into the continuum.

In a two-step description, the transition probability of the Auger decay can be computed as:

$$\mathcal{P}_{i\to f} = \sum_k \frac{2\pi}{\hbar}|M_k'|^2\delta(E_i - E_f)$$
(2.2.3)

This expression makes it evident that the approach decouples the two processes from one another, with the core hole fully relaxing before the Auger decay occurs. It is reasonable to apply this strategy to situations where the laser pulse is ultra short, i.e. interacts with the core hole on a timescale shorter than the Auger decay one.

However, in this work we are interested in the regime where the laser pulse is short but where its interaction with the core level is comparable to the Auger decay timescales. One then needs to consider the one-step approach, where the two events are not assumed to occur separately.

There are many interesting situations where the one-step treatment needs to be applied, for example resonant Auger decay, Auger-photoemission coincidence spectroscopy (APECS) and Auger decay from transition metals (where incomplete screening occurs) to mention a few. The theory behind the one-step approach is considerably more advanced than the two-step treatment. In a rather general form, it was discussed by Almbladh[17] and Gunnarson and Schönhammer[18]. One way to proceed is through the quadratic response formalism, which is naturally expressed in Green's functions language in the frequency domain. However, knowledge and use of Green's functions as a theoretical tool is beyond the scope of this bachelor thesis, and a description of the one-step approach based on them will not be pursued. Given that this thesis deals with a real-time description of the Auger decay, such omission is of little consequence.

2.2.1 Energy vs Time Domain

Indeed, a real-time formulation as given here, where one is describing how the state of the system evolves in time, can be advantageous over a standard energy-picture one-step description: it accounts seamlessly, completely, and in an equal-footing way for all excitation and incomplete screening mechanisms (e.g. shake-up and shake-down contribution, excitonic and plasmonic screening) which occur during the Auger process. This is especially important if one wishes to describe time resolved pump and probe experiments, or specific modulations of the photo-excitation field (e.g. considering train of pulses versus single pulse or constant fields, etc.).

And, ultimately, the standard description of the Auger decay in the energy domain can be recovered by a Fourier analysis of the results obtained in the time domain.

Chapter 3

Time-Dependent Wavefunctions and Computational Real-Time Dynamics

We provide a short background to time-dependent quantum mechanics and numerical integration methods for the Schrödinger equation for systems out of equilibrium. These notions are preliminary ingredients for a real time description of the Auger decay in terms of many-body wavefunctions.

3.1 Exact Diagonalization

The time-dependent Shrödinger equation reads:

$$H \left| \psi \right\rangle = i \frac{d}{dt} \left| \psi \right\rangle .$$ (3.1.1)

If H, the Hamiltonian, is time-independent, the solution is given by[19]:

$$\left| \psi(t) \right\rangle = e^{-iHt} \left| \psi_0 \right\rangle$$ (3.1.2)

Furthermore, with a complete set of basis states in the inherent Hilbert space one can use the completeness relation:

$$\mathbf{1} = \sum_{\lambda} \left| \lambda \right\rangle \left\langle \lambda \right| ,$$ (3.1.3)

and insert a complete set of eigenstates of H in equation 3.1.2:

$$\left| \psi(t) \right\rangle = e^{-iHt} \mathbf{1} \left| \psi_0 \right\rangle = \sum_{\lambda} e^{-iHt} \left| \lambda \right\rangle \left\langle \lambda \right| \left| \psi_0 \right\rangle = \sum_{\lambda} e^{-iE_{\lambda} t} \left| \lambda \right\rangle \left\langle \lambda | \psi_0 \right\rangle$$ (3.1.4)

Thus one can determine the time dependent state vector $\left| \psi(t) \right\rangle$ in terms of the eigenstates of H and the corresponding eigenvalues. Although straightforward, this method involves the diagonalization of the matrix H; if $\dim(H)$, for a particular system, is very large this process becomes time-consuming and ineffective.

If, additionally, the Hamiltonian is time-dependent, then equation 3.1.4, and hence the evolution, must be made recursive and discrete. The state at time $t + dt$ is obtained from the state at time t using equation 3.1.4 with $H \equiv H(t + dt/2)$, valid when dt is small enough so that $H(t)$ is close enough to $H(t + dt)$:

$$|\psi(t + dt)\rangle = \sum_\lambda e^{-iE_\lambda(t+dt/2)dt} |\lambda\rangle \langle\lambda|\psi_0\rangle \tag{3.1.5}$$

As with the case of time-independent Hamiltonians this procedure too becomes very expensive, in fact even more so, for large systems and/or long time propagation since this method involves diagonalizing the Hamiltonian at *each* time step.

3.2 Iterated Lanczos Algorithm

One can work around the problem previously mentioned by means of the iterated Lanczos algorithm[20]. This algorithm is similar to the power method for finding extreme eigenvectors and eigenvalues but uses the Lanczos basis, the basis of the highest order Krylov subspace that is not invariant, to tridiagonalize the matrix A. The definition for a Krylov subspace of rank m, to the range of A with seed v_0 is:

$$\mathcal{K}^m(v_0) = \text{span}\{v_0, Av_0, A^2v_0, ..., A^{k-1}v_0\}.$$

3.2.1 Procedure

Given a starting vector (the seed), v_0 of norm 1 and a hermitian matrix A, multiplying v_0 by A will produce, in general, a new vector $\tilde{q}_1$. Using the Gram-Schmidt process to orthogonalize $\tilde{q}_1$ and v_0 one gets:

$$\tilde{q}_1 = Av_0, \ q_1 = \tilde{q}_1 - \langle v_0|Av_0\rangle v_0 = \tilde{q}_1 - \alpha_0 v_0.$$

After normalizing q_1 we have the second basis vector, v_1, in the Lanczos basis. Multiplying v_1 again by A we get a new vector that we orthogonalize against the previous ones:

$$v_1 = \frac{q_1}{\beta_1}, \ \beta_1 = \|q_1\|$$

$$\tilde{q}_2 = Av_1, \ q_2 = \tilde{q}_2 - \langle v_1|Av_1\rangle v_1 - \langle v_0|Av_1\rangle v_0 = \tilde{q}_2 - \alpha_1 v_1 - \beta_1 v_0.$$

Again, normalizing q_2 and we have the third basis vector of the Lanczos basis, v_2.

$$v_2 = \frac{q_2}{\beta_2}, \ \beta_2 = \|q_2\|.$$

This time around, when producing q_3, something peculiar happens:

$$q_3 = Av_2 - \alpha_2 v_2 - \beta_2 v_1 - \langle v_2|Av_0\rangle v_0.$$

But we know that v_2 has no components parallel to v_0 and v_1 because of the step involving the Gram-Schmidt process, orthogonalizing v_2 to v_0 and v_1, and hence the projection of Av_0 along v_2 is zero:

$$q_3 = Av_2 - \alpha_2 v_2 - \beta_2 v_1 \rightarrow v_3 = \frac{q_3}{\beta_3}.$$

This procedure is entirely general and so we get a recursion formula for the vectors in the Lanczos basis:

$$v_{n+1} = Av_n - \alpha_n v_n - \beta_n v_{n-1} \tag{3.2.1}$$

$$\alpha_n = \langle v_n | Av_n \rangle \tag{3.2.2}$$

$$\beta_n = \|q_n\| = \langle v_{n-1} A | v_n \rangle \tag{3.2.3}$$

If the rank of the matrix A is M, then the maximum number of Lanczos vectors is M. If the Krylov subspaces starts becoming invariant for some smaller $j < M$, i.e. $\mathcal{K}^j(v_0) = \mathcal{K}^{j+1}(v_0)$, then the algorithm should stop as the following α's and β's will be trivially equal to 0 implying that the algorithm will produce undefined behavior when normalize the next vector. The resulting tridiagonal matrix T in the Lanczos basis $\{v_0, v_1, v_2, v_3, ..., v_k\}$ is then:

$$T = \begin{bmatrix} \alpha_0 & \beta_1 & 0 & 0 & \cdots & \cdots \\ \beta_1 & \alpha_1 & \beta_2 & 0 & \cdots & \cdots \\ 0 & \beta_2 & \alpha_2 & \beta_3 & \cdots & \cdots \\ 0 & 0 & \beta_3 & \alpha_3 & \cdots & \cdots \\ \vdots & \vdots & \vdots & \vdots & \ddots & \\ \vdots & \vdots & \vdots & \vdots & & \ddots \end{bmatrix}$$

If the order of the Krylov space is equal to the rank of the original matrix then the eigenvalues of T are exactly those of A since eigenvalues are independent of the basis, and for lower orders the extreme eigenvalues can be obtained to good accuracy. The eigenvectors v of A can be expressed as eigenvectors, v_l, of T through a change of basis back to the original one:

$$\boldsymbol{v_i} = Q\boldsymbol{v_{li}}, \tag{3.2.4}$$

where Q is the $M \times j$ matrix with the Lanczos vectors as columns.

3.2.2 Connection to Exact Diagonalization

From equation 3.1.2 we see that the state vector of the system evolves as an exponential matrix times the ground state. An exponential matrix is defined as:

$$e^{-iAt} = \sum_k \frac{(-it)^k}{k!} A^k \tag{3.2.5}$$

This implies, along with equation 3.1.2:

$$|\psi(t)\rangle = e^{-iHt}|\psi_0\rangle = \sum_{k=0}^{\infty} \frac{(-it)^k}{k!} H^k |\psi_0\rangle \tag{3.2.6}$$

In equation 3.2.6 we can see that the space of states is spanned by the infinite sequence: $\{|\psi_0\rangle, H|\psi_0\rangle, H^2|\psi_0\rangle, H^3|\psi_0\rangle, ...\}$, but from the Lanczos algorithm we found an orthonormal sequence that spanned the same space. So in the Lanczos basis, equation 3.2.6 becomes:

$$|\psi(t)\rangle = \sum_{k}^{M_L} |v_k\rangle \langle v_k| e^{-iH_L t} |v_0\rangle, \tag{3.2.7}$$

where H_L is the tridiagonal matrix obtained from the Lanczos algorithm, M_L is the order of the maximum Krylov subspace and the v_k's are the Lanczos vectors. M_L is less than or equal to M, the dimension of the Hilbert space, but could still be very large so inserting a complete set of states in equation 3.2.6 does not necessarily make the problem any smaller, but considering that the Lanczos algorithm approximates extreme eigenvalues well, a good approximation to equation 3.2.6 is to limit the dimensions of the Lanczos Hamiltonian to some K. This K would have to be determined through trial and error by checking when the results it produces converges to machine accuracy. Once K is chosen, inserting a complete set of eigenstates $\{|\lambda\rangle\}$ in this smaller space with Hamiltonian $H_L^{(K)}$:

$$|\psi(t)\rangle = \sum_{k}^{K} |v_k\rangle \langle v_k| e^{-iH_L^{(K)} t} |v_0\rangle = \sum_{k}^{K} \sum_{\lambda} |v_k\rangle \langle v_k| e^{-iH_L^{(K)} t} |\lambda\rangle \langle \lambda|v_0\rangle = \tag{3.2.8}$$

$$= \sum_{k}^{K} \sum_{\lambda} |v_k\rangle \langle v_k|\lambda\rangle e^{-iE_\lambda t} \langle \lambda|v_0\rangle \tag{3.2.9}$$

3.3 Concurrence

For pure states, states that correspond to vectors in the Hilbert space[19], entanglement is the notion of the state being inseparable into tensor-products of substates[19]. For mixed states being statistical mixtures of pure states the notion is extended as follows: if the pure states, that make up the mixed state are inseparable, i.e. entangled, then so is the mixed state. Mixed states are described by the density operator[19] which can be generically written as:

$$\hat{\rho} = \sum_{i} |\psi_i\rangle \langle \psi_i| \tag{3.3.1}$$

A convenient measure of the separability of a state is that of concurrence, $\mathcal{C}$[21], defined as:

$$\mathcal{C}(\rho) = \max(0, \sqrt{\lambda_1} - \sqrt{\lambda_2} - \sqrt{\lambda_3} - \sqrt{\lambda_4}) \tag{3.3.2}$$

where the λ_i are the decreasing eigenvalues of the 4×4 matrix formed by $\rho\tilde{\rho}$ and ρ is the reduced density matrix given by:

$$\rho = \langle a_{i\sigma}^\dagger a_{j\sigma'}^\dagger a_{k\sigma''} a_{l\sigma'''} \rangle \tag{3.3.3}$$

for fixed i, j, k, l. and $\tilde{\rho}$ is the spin-flipped reduced density matrix:

$$\tilde{\rho} = (\sigma_y \otimes \sigma_y)\rho^*(\sigma_y \otimes \sigma_y) \tag{3.3.4}$$

$\mathcal{C}$ can then be interpreted as a measure of inseparability with values varying between 0 for parallel-spin $|\uparrow\uparrow\rangle$, being unentangled and completely separable, and 1 for anti parallel-spin configurations: $(|\uparrow\downarrow\rangle - |\downarrow\uparrow\rangle)/\sqrt{2}$ which are maximally entangled.

Chapter 4

System and Observables

In this work we investigate a six-electron model of an atomic system that can undergo Auger decay, a minimal model to address and study the coexistence of anti parallel- and parallel- Auger+photoelectron spin configurations. The system consists of three atomic levels $|c\rangle$, $|v_1\rangle$, $|v_2\rangle$, each with s-symmetry, and two continua, X and A both also with s-symmetry. The Hamiltonian for the system in presence of an external light field, in the second quantization formalism, of the system is: $H(t) = H_0 + H_1(t)$, where:

$$H_0 = \sum_\sigma \left[\epsilon_0 \hat{n}_{0\sigma} + \epsilon_1 \hat{n}_{1\sigma} + \epsilon_2 \hat{n}_{2\sigma} \right] + \sum_{i,j=0,\sigma\sigma'}' U_{ij} \hat{n}_{i\sigma} \hat{n}_{j\sigma'} \tag{4.0.1}$$

$$+ \sum_{q \in X, \sigma} \epsilon_q \hat{n}_{q\sigma} + \sum_{k \in A,\ \sigma} \epsilon_k \hat{n}_{k\sigma} + \sum_{qk,\sigma\sigma'} U_{kq} \hat{n}_{k\sigma} \hat{n}_{q\sigma'} + \sum_{i,\ j=1,\sigma\sigma'}^{2}{}' M_{kij}(a_{k\sigma}^\dagger a_{0\sigma'}^\dagger a_{i\sigma'} a_{j\sigma} + \text{H.c.}).$$

Here, the indices 0, 1, 2, label the core level, valence level 1 and valence level 2 respectively, labeling the atomic levels while k and q label the levels in the Auger continua and photo continua, respectively. Also, $\hat{n}_{i\sigma} = a_{i\sigma}^\dagger a_{i\sigma}$ is the number operator for state i with spin projection σ, and the creation/annihilation operators $a_i^\dagger / a_i$ have their usual meaning. The ϵ_i's are the energies of the levels. H_0 describes the internal atomic system, the continua and the interactions M_{kij} which henceforth, as an approximation, are taken to be independent of k: M_{ij}. Finally, a phenomenological interaction, $U_{kq} = K/(\sqrt{\epsilon_k} - \sqrt{\epsilon_q})^2$, is introduced between the photoelectron and the Auger electron where ϵ_q and ϵ_k are their respective energies. The primed sums indicate that terms with $i = j$ and $\sigma = \sigma'$, simultaneously, are excluded.

In the occupation number picture, a general basis state vector, for this model, is given by $|\psi\rangle = |i_1, i_2, i_3; j_1, j_2, j_3\rangle$ where each of the i's labels a generic (either discrete or continuum) one particle state in i with spin projection $+\frac{1}{2}$ and the j's states with spin projection $-\frac{1}{2}$. The state are conventionally ordered in ascending order. In short,

$$|i_1, i_2, i_3; j_1, j_2, j_3\rangle \equiv a_{i_1\uparrow}^\dagger a_{i_2\uparrow}^\dagger a_{i_3\uparrow}^\dagger a_{j_1\downarrow}^\dagger a_{j_2\downarrow}^\dagger a_{j_3\downarrow}^\dagger |vac\rangle.$$

$H_1(t)$ describes the time-dependent (laser) light field that couples the core level to the X-continua:

$$H_1(t) = e^{-\frac{(t-t_0)^2}{2c^2}} \cos(\omega t) \sum_{q \in X, \, \sigma} A_q (a_{q\sigma}^\dagger a_{0\sigma} + \text{H.c.}), \qquad (4.0.2)$$

where the Gaussian prefactor shapes the pulse in the interval $t \in [0, 2t_0]$ and A_q governs the strength of the coupling which is taken to be q independent and identically equal to A_X. The frequency $\nu = 2\pi\omega$ is assumed to be the close to the frequency corresponding to the ionization potential of the atom.

Together, H_0 and $H_1(t)$, describe the dynamics of photoemission followed by an Auger decay. In this framework, the time-dependent Shrödinger equation is solved, with the help of iterating the Lanczos Algorithm, for the time-dependent densities of the atomic levels; $n_{0\sigma}(t), \; n_{1\sigma}(t), \; n_{2\sigma}(t)$ as well as the populations in the continua: $\mathcal{A}(\epsilon_q, t), \; \mathcal{A}(\epsilon_k, t)$.

In general, the size, i.e. the number of configurations, of this problem is $\binom{N_X + N_A + 3}{3}^2$ which quickly becomes quite unmanageable in terms of computer power and time. In order to proceed, we consider an approximation where only configurations that have at most two electrons in the continua, specifically at most one in the photo-continuum and at most one in the Auger-continuum. One can justify this approximation in cases where the laser pulse is ultra short so that the electron that fills the core hole as a result of the Auger decay is not affected by the laser. Figure 3.1-3.3 show the states that are allowed and those that are discarded as a result of this approximation. The ground state is obvious, 6 electrons in the atomic part of the system with 0 in either of the continua. For a state with 5 electrons in the atom, the free electron can only be in the photo-continua since the final state of a photoemission leaves one electron in the X-continuum, and one electron in the Auger continuum is not allowed since photoemission must have occurred before. A state with two free electrons must have one electron in the photo-continuum and one in the Auger-continuum. However, the atomic part cannot be arbitrary, for example a state with no electrons in the core level is out of the game because the probability of a double ionization is very low, especially considering a short pulse. After further deduction (see the figures), the states that are allowed in this approximation are reported next using three different notations, with a total number of states: $N_{states} = 10N_X N_A + 2N_X + 1$. The leftmost expressions will be used henceforth.
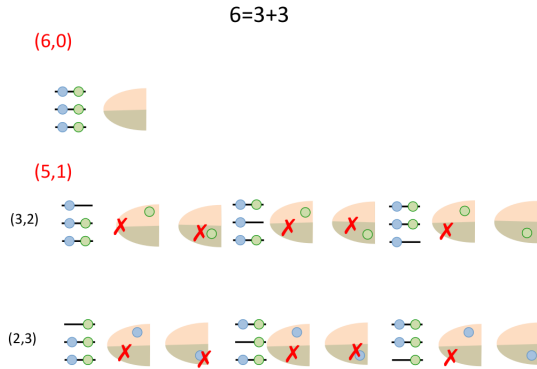
6=3+3

Figure 4.0.1: Possible states with 6 atomic electrons and 0 in either continua, respectively 5 electrons in the atom and 1 in the photo-continua.
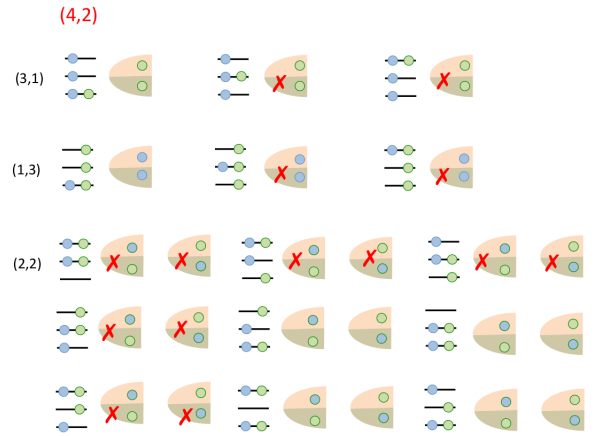

Figure 4.0.2: Possible states with 4 atomic electrons and 2 in the continua.
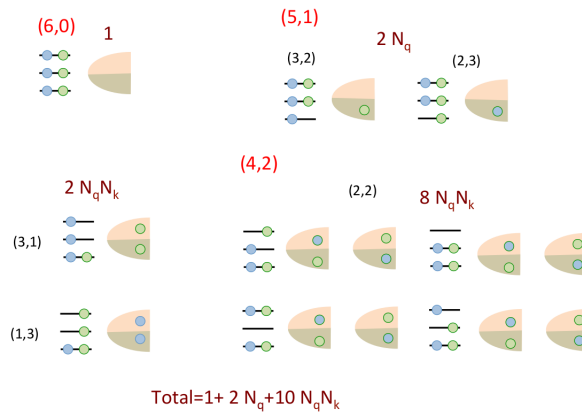

Total=1+ 2 N_q+10 $N_q N_k$

Figure 4.0.3: All *allowed* states and number of permutations allowed for each configurations.

Accordingly, we can label the full set of retained states as (see Figures 4.0.1-4.0.3),

$$|0\rangle = |\psi_0\rangle = |0,1,2;0,1,2\rangle = a_{0\uparrow}^\dagger a_{1\uparrow}^\dagger a_{2\uparrow}^\dagger a_{0\downarrow}^\dagger a_{1\downarrow}^\dagger a_{2\downarrow}^\dagger |vac\rangle$$

$$q \in X : \begin{cases} |q_\uparrow\rangle = |1,2,q;0,1,2\rangle = a_{1\uparrow}^\dagger a_{2\uparrow}^\dagger a_{q\uparrow}^\dagger a_{0\downarrow}^\dagger a_{1\downarrow}^\dagger a_{2\downarrow}^\dagger |vac\rangle \\ |q_\downarrow\rangle = |0,1,2;1,2,q\rangle = a_{0\uparrow}^\dagger a_{1\uparrow}^\dagger a_{2\uparrow}^\dagger a_{1\downarrow}^\dagger a_{2\downarrow}^\dagger a_{q\downarrow}^\dagger |vac\rangle \end{cases}$$

$$q \in X, k \in A : \begin{cases} |A_{11}; q_\uparrow k_\downarrow\rangle = |0,1,q;0,1,k\rangle = a_{0\uparrow}^\dagger a_{1\uparrow}^\dagger a_{q\uparrow}^\dagger a_{0\downarrow}^\dagger a_{1\downarrow}^\dagger a_{k\downarrow}^\dagger |vac\rangle \\ |A_{12}; q_\uparrow k_\downarrow\rangle = |0,1,q;0,2,k\rangle = a_{0\uparrow}^\dagger a_{1\uparrow}^\dagger a_{q\uparrow}^\dagger a_{0\downarrow}^\dagger a_{2\downarrow}^\dagger a_{k\downarrow}^\dagger |vac\rangle \\ |A_{21}; q_\uparrow k_\downarrow\rangle = |0,2,q;0,1,k\rangle = a_{0\uparrow}^\dagger a_{2\uparrow}^\dagger a_{q\uparrow}^\dagger a_{0\downarrow}^\dagger a_{1\downarrow}^\dagger a_{k\downarrow}^\dagger |vac\rangle \\ |A_{22}; q_\uparrow k_\downarrow\rangle = |0,2,q;0,2,k\rangle = a_{0\uparrow}^\dagger a_{2\uparrow}^\dagger a_{q\uparrow}^\dagger a_{0\downarrow}^\dagger a_{2\downarrow}^\dagger a_{k\downarrow}^\dagger |vac\rangle \\[6pt] |A; q_\uparrow k_\uparrow\rangle = |0,q,k;0,1,2\rangle = a_{0\uparrow}^\dagger a_{q\uparrow}^\dagger a_{k\uparrow}^\dagger a_{0\downarrow}^\dagger a_{1\downarrow}^\dagger a_{2\downarrow}^\dagger |vac\rangle \\[6pt] |A_{11}; q_\downarrow k_\uparrow\rangle = |0,1,k;0,1,q\rangle = a_{0\uparrow}^\dagger a_{1\uparrow}^\dagger a_{k\uparrow}^\dagger a_{0\downarrow}^\dagger a_{1\downarrow}^\dagger a_{q\downarrow}^\dagger |vac\rangle \\ |A_{12}; q_\downarrow k_\uparrow\rangle = |0,1,k;0,2,q\rangle = a_{0\uparrow}^\dagger a_{1\uparrow}^\dagger a_{k\uparrow}^\dagger a_{0\downarrow}^\dagger a_{2\downarrow}^\dagger a_{q\downarrow}^\dagger |vac\rangle \\ |A_{21}; q_\downarrow k_\uparrow\rangle = |0,2,k;0,1,q\rangle = a_{0\uparrow}^\dagger a_{2\uparrow}^\dagger a_{k\uparrow}^\dagger a_{0\downarrow}^\dagger a_{1\downarrow}^\dagger a_{q\downarrow}^\dagger |vac\rangle \\ |A_{22}; q_\downarrow k_\uparrow\rangle = |0,2,k;0,2,q\rangle = a_{0\uparrow}^\dagger a_{2\uparrow}^\dagger a_{k\uparrow}^\dagger a_{0\downarrow}^\dagger a_{2\downarrow}^\dagger a_{q\downarrow}^\dagger |vac\rangle \\[6pt] |A; q_\downarrow k_\downarrow\rangle = |0,1,2;0,q,k\rangle = a_{0\uparrow}^\dagger a_{1\uparrow}^\dagger a_{2\uparrow}^\dagger a_{0\downarrow}^\dagger a_{q\downarrow}^\dagger a_{k\downarrow}^\dagger |vac\rangle , \end{cases}$$

Here, in the third subset of basis states, the A_{ij}:s denote the atomic configuration in the final state ("A" stands for "atom"), with i and j each denoting a *hole* in one of the valence levels. So the notation makes explicit the distribution of electrons between atomic and continua levels. We wish to stress that in this basis subset, core levels are doubly filled, and their indexes never appear. [1]

A general state of the system can thus be written as a linear combination of these states:

$$|\Psi(t)\rangle = \alpha_0(t) |0\rangle + \sum_{q \in X} \Big[\alpha_{q\uparrow}(t) |q_\uparrow\rangle + \alpha_{q\downarrow}(t) |q_\downarrow\rangle + \sum_{k \in A} \sum_{i,j=1}^{2} b_{kq}^{\uparrow\downarrow}(i,j;t) |A_{ij}; q_\uparrow k_\downarrow\rangle +$$
$$+ b_{kq}^{\downarrow\uparrow}(i,j;t) |A_{ij}; q_\downarrow k_\uparrow\rangle + c_{kq}^{\uparrow\uparrow}(t) |A_{12}; q_\uparrow k_\uparrow\rangle + c_{kq}^{\downarrow\downarrow}(t) |A_{12}; q_\downarrow k_\downarrow\rangle \Big], \tag{4.0.3}$$

where i and j again label holes in the atomic valence levels 1 and 2.

In this basis, a result of our truncation of the Hilbert space, there are physical states intentionally left out. For example, one such state could be where both core electrons are photoemitted followed by two Auger decays filling the two core holes: this would lead to states like $|q_\uparrow q_\downarrow\rangle$ and $|q_\uparrow k_\uparrow q_\downarrow k_\downarrow\rangle$ being included. These states are left out in part because (as was mentioned before) of

---

[1]Note that, despite the photoelectron and Auger electron having opposite spin projections they need not be in a singlet state, for example $(|\uparrow\downarrow\rangle + |\downarrow\uparrow\rangle)/\sqrt{2}$ is a triplet state, but the spin projections are anti parallel.

their negligible contribution for very short pulses, but also because they expand the Hilbert space to $(N_X N_A)^2$ which would quickly scale out of reach.

With the ordering convention used for the states, care must be taken with relative phases, in particular the signs of the matrix elements must be determined in order to have an accurate model. The calculations for M_{ij} are hence given below:

$$
\begin{aligned}
M_{11} \langle A_{11}; q_\uparrow k_\downarrow| \, a_{k\downarrow}^\dagger a_{0\uparrow}^\dagger a_{1\uparrow} a_{1\downarrow} \, |q_\uparrow\rangle = \\
= M_{11} \langle A_{11}; q_\uparrow k_\downarrow| a_{k\downarrow}^\dagger a_{0\uparrow}^\dagger a_{1\uparrow} a_{1\downarrow} a_{1\uparrow}^\dagger a_{2\uparrow}^\dagger a_{q\uparrow}^\dagger a_{0\downarrow}^\dagger a_{1\downarrow}^\dagger a_{2\downarrow}^\dagger |v\rangle = \\
= M_{11} \langle A_{11}; q_\uparrow k_\downarrow| \, a_{k\downarrow}^\dagger a_{0\uparrow}^\dagger (-1)^4 a_{2\uparrow}^\dagger a_{q\uparrow}^\dagger a_{0\downarrow}^\dagger a_{2\downarrow}^\dagger \, |v\rangle = \\
= M_{11} \langle A_{11}; q_\uparrow k_\downarrow|(-1)^9 a_{0\uparrow}^\dagger a_{2\uparrow}^\dagger a_{q\uparrow}^\dagger a_{0\downarrow}^\dagger a_{2\downarrow}^\dagger a_{k\downarrow}^\dagger |v\rangle = -M_{11} \cdot \langle A_{11}; q_\uparrow k_\downarrow|A_{11}; q_\uparrow k_\downarrow\rangle = -M_{11}
\end{aligned}
\tag{4.0.4}
$$

Similarly, for the other states:

$$
M_{12} \langle A_{12}; q_\uparrow k_\downarrow| \, a_{k\downarrow}^\dagger a_{0\uparrow}^\dagger a_{1\uparrow} a_{2\downarrow}|q_\uparrow\rangle = M_{12}
\tag{4.0.5}
$$

$$
M_{21} \langle A_{21}; q_\uparrow k_\downarrow|a_{k\downarrow}^\dagger a_{0\uparrow}^\dagger a_{2\uparrow} a_{1\downarrow}|q_\uparrow\rangle = M_{21}
\tag{4.0.6}
$$

$$
M_{22} \langle A_{22}; q_\uparrow k_\downarrow|a_{k\downarrow}^\dagger a_{0\uparrow}^\dagger a_{2\uparrow} a_{2\downarrow}|q_\uparrow\rangle = -M_{22}
\tag{4.0.7}
$$

$$
M_{12} \langle A; q_\uparrow k_\uparrow|a_{k\uparrow}^\dagger a_{0\uparrow}^\dagger a_{1\uparrow} a_{2\uparrow}|q_\uparrow\rangle = -M_{12}
\tag{4.0.8}
$$

$$
M_{21} \langle A; q_\uparrow k_\uparrow|a_{k\uparrow}^\dagger a_{0\uparrow}^\dagger a_{2\uparrow} a_{1\uparrow}|q_\uparrow\rangle = M_{21}
\tag{4.0.9}
$$

The structure of the calculations for flipped spins is analogous, and since there are no spin-flipping terms in the Hamiltonian they are not written explicitly here, but are of course included in the calculations. We can see that M_{11}, M_{12}, M_{21}, M_{22} all contribute to anti parallel-spin configurations while $-M_{12} + M_{21}$ is responsible for parallel-spin configurations.

In order to examine the concurrence in the final state between the photoelectron and the Auger electron we now turn to the reduced density matrix, ρ_{kq}:

$$
\rho_{kq} \stackrel{def}{=} \langle a_{k\sigma_1}^\dagger a_{q\sigma_2}^\dagger a_{q\sigma_3} a_{k\sigma_4}\rangle
\tag{4.0.10}
$$

The matrix in 4.0.11 shows how the values of the σ_i are chosen, the values of σ_1 and σ_2 change between rows, and the values of σ_3 and σ_4 change between columns.

$$
\begin{array}{c}
\begin{array}{cccc}
\uparrow\uparrow & \uparrow\downarrow & \downarrow\uparrow & \downarrow\downarrow
\end{array} \\
\begin{array}{c}
\uparrow\uparrow \\
\uparrow\downarrow \\
\downarrow\uparrow \\
\downarrow\downarrow
\end{array}
\left(
\begin{array}{cccc}
\rho_{11} & \rho_{12} & \cdots & \rho_{14} \\
\rho_{21} & \rho_{22} & \cdots & \rho_{24} \\
\vdots & \vdots & \ddots & \vdots \\
\rho_{41} & \rho_{42} & \cdots & \rho_{44}
\end{array}
\right)
\end{array}
\tag{4.0.11}
$$

As is clear from the structure of the Hamiltonian, $[H, S_z] = 0$ and $[H, \boldsymbol{S}^2] = 0$, and hence only elements with $\sigma_1 = \sigma_4$ and $\sigma_2 = \sigma_3$, or $\sigma_1 = -\sigma_4$ and $\sigma_2 = -\sigma_3$ will give non-zero elements:

16

$$\rho_{11} = \alpha = \langle \Psi | a_{k\uparrow}^\dagger a_{q\uparrow}^\dagger a_{q\uparrow} a_{k\uparrow} | \Psi \rangle = + |c_{kq}^{\uparrow\uparrow}|^2 \tag{4.0.12}$$

$$\rho_{22} = \beta = \langle \Psi | a_{k\uparrow}^\dagger a_{q\downarrow}^\dagger a_{q\uparrow} a_{k\downarrow} | \Psi \rangle = + \sum_{i,j=1}^{2} |b_{kq}^{\downarrow\uparrow}(i,j)|^2 \tag{4.0.13}$$

$$\rho_{23} = \gamma = \langle \Psi | a_{k\uparrow}^\dagger a_{q\downarrow}^\dagger a_{q\downarrow} a_{k\uparrow} | \Psi \rangle = + \sum_{i,j=1}^{2} |b_{kq}^{\downarrow\uparrow}(i,j)|^2 \tag{4.0.14}$$

$$\rho_{33} = \beta = \langle \Psi | a_{k\downarrow}^\dagger a_{q\uparrow}^\dagger a_{q\downarrow} a_{k\uparrow} | \Psi \rangle = + \sum_{i,j=1}^{2} |b_{kq}^{\uparrow\downarrow}(i,j)|^2 \tag{4.0.15}$$

$$\rho_{32} = \gamma = \langle \Psi | a_{k\downarrow}^\dagger a_{q\uparrow}^\dagger a_{q\uparrow} a_{k\downarrow} | \Psi \rangle = + \sum_{i,j=1}^{2} |b_{kq}^{\uparrow\downarrow}(i,j)|^2 \tag{4.0.16}$$

$$\rho_{44} = \alpha = \langle \Psi | a_{k\downarrow}^\dagger a_{q\downarrow}^\dagger a_{q\downarrow} a_{k\downarrow} | \Psi \rangle = + |c_{kq}^{\downarrow\downarrow}|^2 \tag{4.0.17}$$

Hence, ρ_{kq} is:

$$
\begin{pmatrix}
\alpha & 0 & 0 & 0 \\
0 & \beta & \gamma & 0 \\
0 & \gamma & \beta & 0 \\
0 & 0 & 0 & \alpha
\end{pmatrix}
\Rightarrow
\begin{pmatrix}
\alpha & 0 & 0 & 0 \\
0 & \beta & \beta & 0 \\
0 & \beta & \beta & 0 \\
0 & 0 & 0 & \alpha
\end{pmatrix}
\tag{4.0.18}
$$

As explained in section 3.3, we want the matrix given by $\rho\tilde{\rho}$:

$$\tilde{\rho} = (\sigma_y \otimes \sigma_y)\rho^*(\sigma_y \otimes \sigma_y) = \rho \implies \rho\tilde{\rho} = \rho^2 \tag{4.0.19}$$

The general result for the eigenvalues of a matrix such as ρ^2 is, by simple pen and paper diagonalization:

$$\lambda_1 = 4\beta^2, \ \lambda_{2,3} = \alpha^2, \lambda_4 = 0. \implies \tag{4.0.20}$$

$$C_{kq}(\rho_{kq}) = \max(0, \sum_{i,j=1}^{2} 2|b_{kq}^{\uparrow\downarrow/\downarrow\uparrow}(i,j)|^2 - 2|c_{kq}^{\uparrow\uparrow/\downarrow\downarrow}|^2) \tag{4.0.21}$$

Because of the way the parallel-spin configuration is reached, with the matrix element $M_{21} - M_{12}$, the maximum value of it is no greater than either of M_{12} or M_{21} and hence:

$$\sum_{i,j=1}^{2} |b_{kq}^{\uparrow\downarrow/\downarrow\uparrow}(i,j)|^2 \geq |c_{kq}^{\uparrow\uparrow/\downarrow\downarrow}|^2 \tag{4.0.22}$$

where i and j label the holes in the valence level of the electron, summing over them because there are multiple configurations that correspond to anti parallel-spin states but only one parallel-spin state with $S = 1$.

In this approximation, neglecting the contribution from double photoemission, the maximum value of the density of either spin channel in the photo-continuum is 0.5, since (assuming no Auger decay has occurred) the system ends up in a superposition of states corresponding to the either of the two spin channels.

$$|\psi_{ph}\rangle = \sum_q \frac{1}{\sqrt{2}}(\alpha_{q\uparrow}|q_\uparrow\rangle + \alpha_{q\downarrow}|q_\downarrow\rangle)$$

(4.0.23)

This property will carry through to the final state, since the Auger term in the Hamiltonian does not affect the photoelectron. That is,

$$\sum_{kq}(|c_{kq}^{\uparrow\uparrow}|^2 + \sum_{i,j=1}^{2}|b_{kq}^{\uparrow\downarrow}(i,j)|^2) \leq \frac{1}{2}$$

(4.0.24)

$$\sum_{kq}(|c_{kq}^{\downarrow\downarrow}|^2 + \sum_{i,j=1}^{2}|b_{kq}^{\downarrow\uparrow}(i,j)|^2) \leq \frac{1}{2}$$

(4.0.25)

From equation 4.0.24 we can see that if the final state is in an anti parallel-spin configuration, i.e. $|c_{kq}^{\uparrow\uparrow/\downarrow\downarrow}|^2 = 0$, the concurrence is equal to 1 indicating that the photoelectron and Auger electron are maximally entangled in accordance with what is expected.

Chapter 5

Results

This thesis is designed to be an exploratory investigation in the time domain of the Auger decay for a simple model atomic system, particularly about the entanglement of photo- and Auger electrons. The dynamics will be tracked by calculating the various atomic densities as well as the continua electron densities. Furthermore, concurrence is calculated at the end of each calculation. The result will be structured into two parts, one where U_{kq} (the Coulomb interaction between photo- and Auger electrons) is kept fixed and the matrix elements M_{12} and M_{21} are varied and the second where the matrix elements are fixed and U_{kq} varies.

Not considering the parallel-spin contribution $(M_{12} - M_{21})^2$ to the transition rate (which clearly depends on the relative value of M_{12} and M_{21}), the total Auger rate is given by: $M^2 = M_{11}^2 + M_{22}^2 + M_{12}^2 + M_{21}^2$. That is then divided into two parts: $\frac{M^2}{2} = M_{11}^2 + M_{22}^2$ and $\frac{M^2}{2} = M_{21}^2 + M_{12}^2$.

Since it is the particular combination $M_{21} - M_{12}$ of the matrix elements M_{12}, M_{21} which is responsible for the parallel spin contribution, M_{11} and M_{22} will be kept fixed with their sum equal to $M^2/2$ throughout while M_{12} and M_{21} will be the ones varied. Table 5.0.1 shows the various relevant parameters, and in the chapter the figure captions will only report deviations from these parameters.

Table 5.0.1: Various Parameters.

E_{core} =	56	E_{v1} =	25	E_{v2} =	15		
U_{00}	5	U_{01}	4	U_{02}	3	$U_{kq} = \frac{K}{(\sqrt{\epsilon_k} - \sqrt{\epsilon_q})^2}$	
U_{11}	5	U_{12}	4	U_{22}	5		
M_{11}	0.0069	M_{12}	0.0075	M_{21}	0.0049	M_{22}	0.0057
A_X	-0.3	N_A	600	N_X	100	ω	87

We mention again at this point that we are investigating the dynamics of a system that is perturbed by a narrow Gaussian wave packet. We are interested in understanding the relationship between the anti parallel-spin configuration and parallel-spin configuration in order to quantify, using concurrence, the degree of entanglement between the spin of the photoelectron and the Auger electron. Firstly we look at a pure photoemission in order to shape the pulse and also to have an understanding of the how the density of electrons in the core level changes over time with no Auger decay involved.
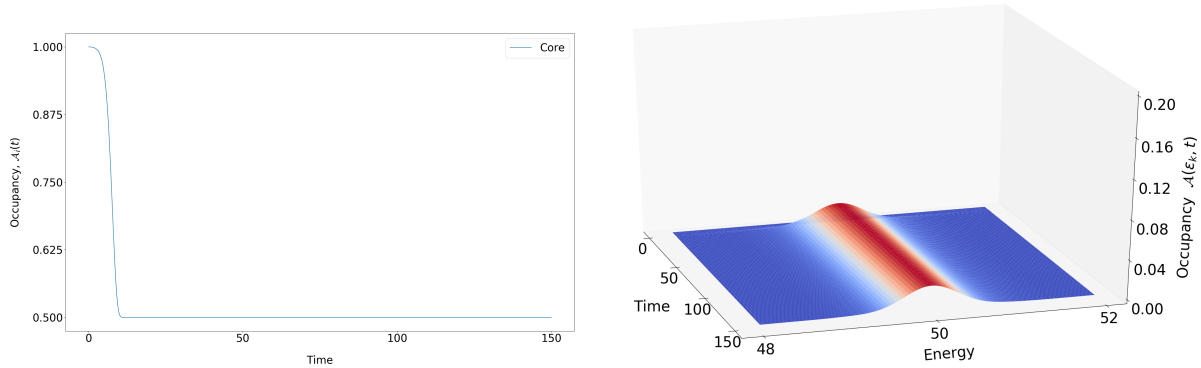
(a) Core level electron density for either spin channel in the presence of an external laser light field, where no Auger decay is allowed.

(b) Electron density in the photo-continuum as a result of ionization from an external laser light field.

Figure 5.0.1: Behavior of the system, under the influence of the external laser light

Figure 5.0.1 panel (a) shows how the density of spin up, or down, electrons in the core level changes as a Gaussian wave packet interacts with the system. The core level is quickly depleted of one electron, i.e. the density of charge in the continuum corresponds to one electron. Because the light field interacts independently on electrons with both spin projections, the state of the system after emission will be a combination of emitted spin-up and spin-down electrons.Panel (b) shows the spectral peak in the photocontinuum.

5.0.1 Fixed U_{kq} with varying matrix elements

The results in figure 5.0.2 show the expectation values of the electron densities $\hat{n}_{k\sigma}(t)$ in the Auger spectra as functions of time and energy. One can see that there are three distinct peaks corresponding to the three different energies of the Auger electron, depending on the configuration of the decay. The lowest energy energy peak corresponds to the Auger electron that was ionized in the decay involving only valence level 1 electrons. This can be understood considering that in this case, from equation 2.2.1 and taking into account atomic interactions, the energy is determined as

$$0 = E(q_{\uparrow/\downarrow}) - E(A_{11}; q_{\uparrow/\downarrow}k_{\downarrow/\uparrow}) \implies$$
$$E_A = 24 \tag{5.0.1}$$

where $E(X)$ denotes the energy of the basis state $|X\rangle$ where $E(q_{\uparrow/\downarrow})$ is the long time limit of the energy of the state where a photoelectron has been emitted, and $E(A_{11}; q_{\uparrow/\downarrow}k_{\downarrow/\downarrow})$ is the long time limit of the energy of the state after the Auger decay leaving to holes in valence level 1. The middle-energy peak is the energy of the Auger electron involved in the Auger decay with different valence level, and the highest-energy peak is the one from the decay involving only valence level 2. Keeping the interaction between the photoelectron and the Auger electron fixed, while varying the matrix elements M_{12} and M_{21} from $M_{12} = M_{21}$ to $M_{12} = M/\sqrt{2}$ and $M_{21} = 0$, one can see that there is no difference in the location in energy of the peaks; however, there is a difference in the density of electrons between the peaks. As the parallel-spin contribution increases, the density of electrons at the energy corresponding to Auger electron emitted in a decay involving both valence levels increases at the expense of the intra-level Auger decays.

Auger Spectra

Figure 5.0.2: Varying the ratio M_{21} to M_{12} in the equation $M_{12}^2 + M_{21}^2 = M^2/2$ through 5:5, 7:3 and 10:0 from top to bottom with $K = 0$.

This is due to the fact that the total Auger rate depends also on $(M_{12} - M_{21})^2$, which is responsible for the parallel-spin contribution to the decay. When $M_{12} \neq M_{21}$, the total Auger rate goes up, adding to the height of the central-energy peak, while the lowest- and highest- energy rates are kept
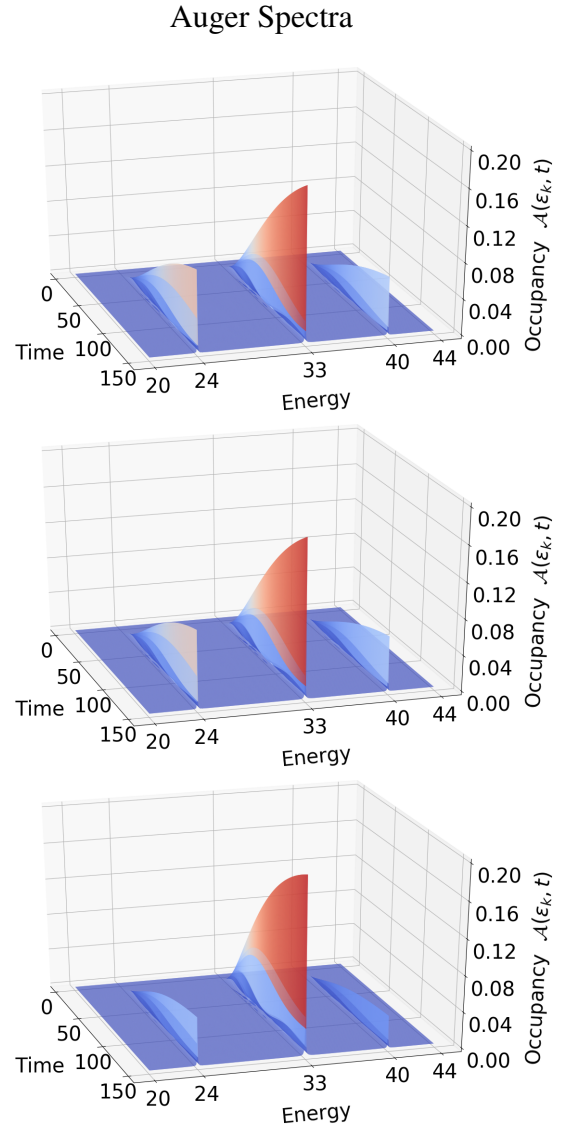
fixed throughout. Thus, the relative strengths of M_{11} and M_{22} are diminished while the combined effect of the anti parallel and parallel-spin parts of M_{12} is increased. We now move to consider the entanglement between photo- and Auger electrons.

On the right, we report the concurrence $\mathcal{C}$ between the photoelectron and the Auger electron as functions of their energies. One can see a clear resemblance between the structure of the peaks here compared to the peaks in the Auger spectra and the photo spectra. As M_{12} and M_{21} are varied, the concurrence between the photoelectron and the Auger electron is diminished (this is evident by looking at the middle peak). Interestingly, and in contrast with the Auger peaks, the concurrence between the photoelectron and the Auger electron decreases as the difference between M_{12} and M_{21} increases. This is because the more likely the parallel-spin configuration is, the less likely the photoelectron and the Auger electron are to have opposite spin. The parallel contribution thus masks the correlation between the spins. Again, the edge peaks can be seen to decrease due to the same phenomenon as in the Auger spectra: when the parallel-spin configuration is increased, the total Auger rate increases at the expense of the contributions from M_{11} and M_{22}, this can be seen clearly from the expression of $\mathcal{C}$ in equation 4.0.21. We can see that the maximum value of the concurrence between two electrons at *specific* energies is around 0.016 however the total concurrence, and the local concurrence for each peak, are significantly higher, as reported in Table 5.0.2.

Table 5.0.2: Table showing the total and local concurrence for each scenario, $\mathcal{C}_{1,2,3}$ refer to the peaks with low, middle and high Auger energy, respectively.

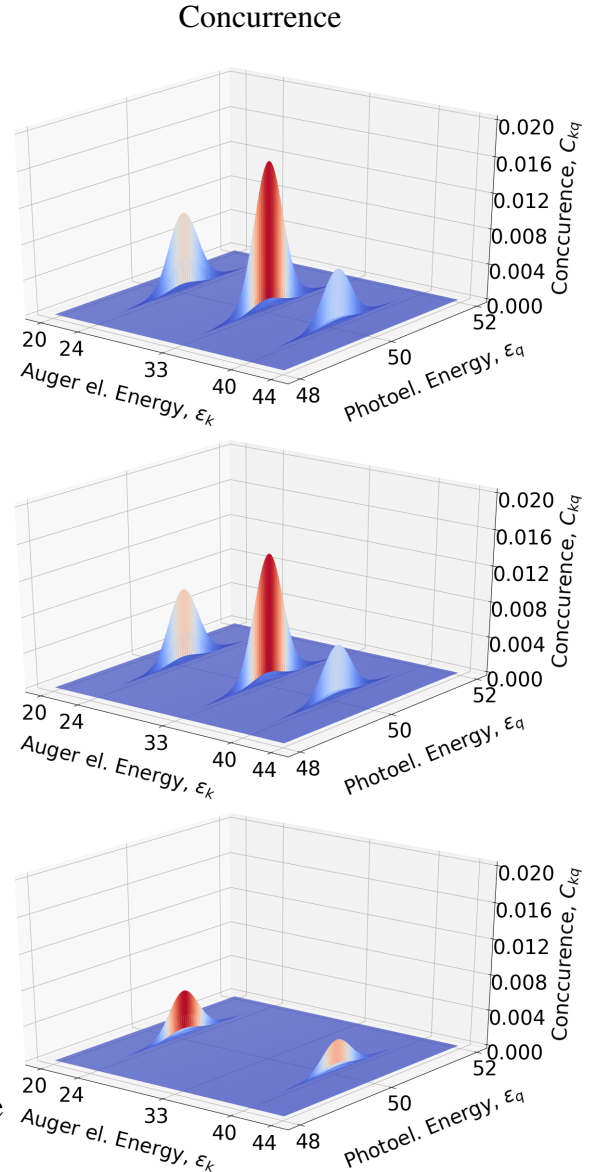|	5:5	7:3	10:0
$\mathcal{C}_{total}$	0.97	0.90	0.34
$\mathcal{C}_1$	0.33	0.32	0.22
$\mathcal{C}_2$	0.47	0.42	0
$\mathcal{C}_3$	0.17	0.16	0.12

Concurrence

Figure 5.0.3: Varying the ratio M_{12} to M_{21} in the equation $M_{12}^2 + M_{21}^2 = M^2/2$, through 5:5, 7:3, 10:0 from top to bottom with $K = 0$.

5.0.2 Fixed matrix elements, with varying U_{kq} interaction

In this column we display results for the concurrence when the interaction U_{kq} varies and all the matrix elements are kept fixed at the values in table 5.0.1. By increasing the strength of the interaction, the concurrence peaks split. Furthermore, their positions on the Auger energy axis are shifted downwards, by different amounts depending on the strength of the interaction and their energy. Because of the type of interaction used, the closer the Auger energy is to the photoelectron energy, the stronger the interaction becomes. This offers a likely explanation for the shift to lower energies. Due to energy conservation before the Auger decay and after, with a repulsive interaction between the electrons in the continuum the total energy increases and hence the energy of the Auger electron must decrease. This is also consistent with the fact that the peaks do not shift by the same amount, since the higher energy peak is closer to the photoelectron energy, thus the interaction is stronger, and the decrease must be greater.

The reason for the peaks splitting could be related to a more nuanced effect of the interaction. A possible mechanism is that, for an ultrashort pulse, the energy of the photoelectron is fixed after the emission and before the Auger decay, and for a relatively broad photo peak the density of charge away from the center energy is relatively large. To conserve energy, the widths of the Auger peaks must also be broadened, and if the photoelectron energy is lower, the energy of the Auger electron also tends to be lower. But here

Concurrence

Figure 5.0.4: Varying U_{kq}, with the matrix elements fixed, with $K =0$, 1, 3 (see column 4 in table 5.0.1).

is the nuance: the interaction depends on the electrons' energies and if the photoelectron energy is lowered as well as the Auger energy, the interaction changes little. Conversely, if the Auger energy does not change, the interaction increases. For a fixed photo energy, the Auger energy can change while at the same time the interaction changes. Since the interaction is more sensitive to changes in Auger energy close to the photoelectron energy, this is could be the reason why the higher energy peak splits more compared to the intermediate and lower energy Auger electron. If the above speculative arguments hold, then it is possible that the modality of the splitting could turn out significantly different for a more realistic interaction. And, for a slower pulse, also be dependent on the competition between the pulse emptying the core level, and the Auger transitions filling it.
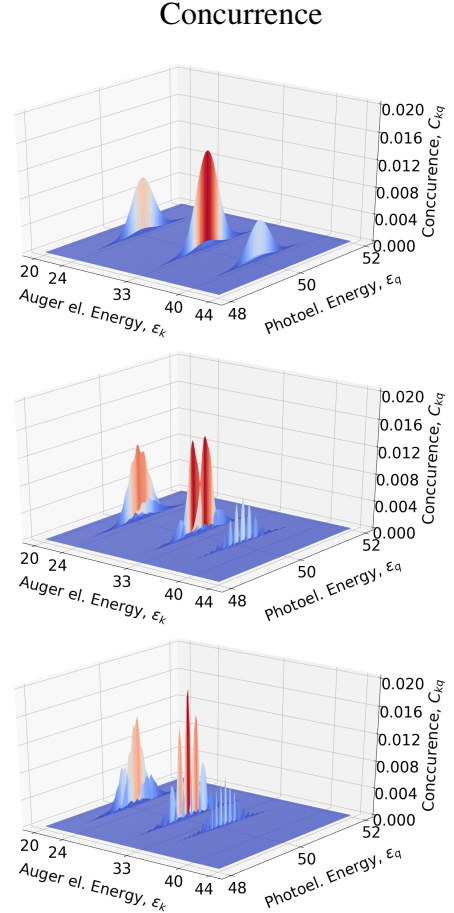
Chapter 6

Conclusion and outlook

We have introduced and computationally implemented a minimal model for a time-dependent description of photoemission and Auger decay in atoms. An uncommon and attractive feature of our method is that it accounts for both photo- and Auger electrons in a coherent, equal footing formulation, by time-evolving the many-body wavefunction of the system. Due to the complexity of the problem, we introduced a truncation of the configuration space, based on a constraint on the total number of electrons ejected from the atom in to the continuum. But, and most importantly, this still fully retains the interplay between the photoelectron and Auger channels.

One merit of our approach is to provide a quite versatile benchmarking tool to more sophisticated treatments. A second clear advantage is that it permits to address at the qualitative level a number of interesting aspects of atomic transitions in the time domain. An example in this respect, and central to this work is the entanglement between photo- and Auger electrons, a topic currently of growing scientific interest. Our work takes a first step in this direction, by studying the time dependent concurrence (a measure of entanglement) in the spin sector. We find that the interactions between the electrons in the continuum strongly affect the modality of entanglement.

As future directions, we mention the following possibilities: i) one could further investigate the interplay of photo- and Auger electron dynamics, specifically from a Bell states perspective.

ii) Due to the different Auger decay channels available in the model, interesting interference effects must result in the temporal features of the decay; these could be characterized via an exploration of the transition rate parameters.

iii) On the more ambitious side, a rather important problem is how to deal with larger configuration spaces, to release the current constraints on the nature of the laser interactions. On speculative ground, it is not unlikely that a hybrid approach would be needed, where e.g the photoelectron continuum is described by a more advanced formalism, e.g. via the Green's function technique.

These possibilities are left for the future, and in concluding we note that our model is simplistic and minimal, and is a tool for preliminary investigations. Nevertheless, the results already found here display interesting aspects of time-resolved atomic processes worth investigating further.

Bibliography

[1] P. Lenard. Ueber die lichtelektrische wirkung. Annalen der Physik, 313(5):149–198, 1902.

[2] D.J. Griffiths. Introduction to Electrodynamics. Pearson Education, 2014.

[3] M Planck. Ueber das gesetz der energieverteilung im normalspectrum. Annalen der Physik, 309(3):553–563, 1901.

[4] A. Einstein. Über einen die erzeugung und verwandlung des lichtes betreffenden heuristischen gesichtspunkt. Annalen der Physik, 322(6):132–148, 1905.

[5] L. Meitner. Über die entstehung der β-strahl-spektren radioaktiver substanzen. Zeitschrift für Physik, 9(1):131–144, Dec 1922.

[6] P. Auger. Sur l'effet photoélectrique composé. J. Phys. Radium, 6(6):205–208, 1925.

[7] M. S. Schöffler, J. Titze, N. Petridis, T. Jahnke, K. Cole, L. Ph. H. Schmidt, A. Czasch, D. Akoury, O. Jagutzki, J. B. Williams, N. A. Cherepkov, S. K. Semenov, C. W. McCurdy, T. N. Rescigno, C. L. Cocke, T. Osipov, S. Lee, M. H. Prior, A. Belkacem, A. L. Landers, H. Schmidt-Böcking, Th. Weber, and R. Dörner. Ultrafast probing of core hole localization in n2. Science, 320(5878):920–923, 2008.

[8] E. Viñas Boström, M. Gisselbrecht, T. Brage, C.-O. Almbladh, A. Mikkelsen, and C. Verdozzi. Time-stretched spectroscopy by the quantum zeno effect: The case of auger decay. Phys. Rev. Lett., 121:233201, Dec 2018.

[9] K. Siegbahn. ESCA : atomic, molecular and solid state structure studied by means of electron spectroscopy. Stockholm, 1967.

[10] R. Horodecki, P. Horodecki, M. Horodecki, and K. Horodecki. Quantum entanglement. Rev. Mod. Phys., 81:865–942, Jun 2009.

[11] J.M. Hollas. Modern Spectroscopy. Wiley, 2004.

[12] Advanced Quantum Mechanics. Springer Berlin Heidelberg, Berlin, Heidelberg, 2008.

[13] G. Grynberg, A. Aspect, C. Fabre, and C. Cohen-Tannoudji. Introduction to Quantum Optics: From the Semi-classical Approach to Quantized Light. Cambridge University Press, 2010.

[14] D. A. Shirley. Relaxation effects on auger energies. Chemical Physics Letters, 17(3):312 – 315, 1972.

[15] P. Weightman. X-ray-excited auger and photoelectron spectroscopy. Reports on Progress in Physics, 45(7):753–814, jul 1982.

[16] D. CHATTARJI. Chapter two - theory of the auger process. In D. CHATTARJI, editor, The Theory of Auger Transitions, pages 13 – 29. Academic Press, 1976.

[17] C.-O. Almbladh. Incomplete relaxation in a model problem for the auger process. Il Nuovo Cimento B, 23(1):76–89, 1974.

[18] O. Gunnarsson and K. Schönhammer. Dynamical theory of auger processes. Phys. Rev. B, 22:3710–3733, Oct 1980.

[19] D.J. Tannor. Introduction to Quantum Mechanics. University Science Books, 2007.

[20] C. Lanczos. An iteration method for the solution of the eigenvalue problem of linear differential and integral operators. J. Res. Natl. Bur. Stand. B, 45:255–282, 1950.

[21] S. Hill and W. K. Wootters. Entanglement of a pair of quantum bits. Phys. Rev. Lett., 78:5022–5025, Jun 1997.

Appendix: The code

This is an original computer source code, completely written from scratch by the author of this thesis, which simulates the time evolution of a model atomic system excited by light, and where an electron emission in the continuum is followed by atomic Auger recombination. The structure of the code is explained in the main text of the thesis. The code is to be used in conjunction with a second code, not shown here, which determines the basis set to be used in the calculations.

```cpp
#include <iostream>
#include <fstream>
#include <xtensor/xarray.hpp>
#include <xtensor/xio.hpp>
#include <xtensor/xview.hpp>
#include <xtensor/xindex_view.hpp>
#include <xtensor-blas/xlinalg.hpp>
#include <tuple>
#include <xtensor/xmanipulation.hpp>
#include <xtensor/xio.hpp>
#include <complex>
#include <xtensor/xarray.hpp>
#include <xtensor/xcomplex.hpp>
#include <vector>
#include <xtensor/xoperation.hpp>
#include <xtensor/xnorm.hpp>
#include <xtensor/xrandom.hpp>
#include <xtensor/xfixed.hpp>
using namespace xt;



void Lanczos(int H_dim, auto states, auto x0, double dt, int nt,
int n_xct, int n_sct){

int L  = H_dim;
int klimit = 7;
double tol = 1e-16;
const std::complex<double> j(0,1);
xarray<std::complex<double>> x_k = x0;
```

```
xarray<std::complex<double>> tridia, > A_base, x_km1, x_kp1, a_k,
b_k, rr, y_tmp, ct, Hx_k, phases0;

int nat = 3;
int norb = nat + n_xct + n_sct;

std::ofstream psi0_file;
psi0_file.open ("Three_level_plot_data.txt");

std::ofstream ent_file_ud, ent_file_uu;
ent_file_ud.open("densitymatrix_ud.txt");
ent_file_uu.open("densitymatrix_uu.txt");

psi0_file << n_xct << std::endl;
psi0_file << n_sct << std::endl;


for (int t = 0; t < nt; t++)
{
tridia = zeros<std::complex<double>>({klimit + 1, klimit + 1});
A_base = zeros<std::complex<double>>({klimit + 1, L});
x_km1 = zeros<std::complex<double>>({L});
x_kp1 = zeros<std::complex<double>>({L});
y_tmp = zeros<std::complex<double>>({L});
a_k = zeros<std::complex<double>>({1});
b_k = zeros<std::complex<double>>({1});
rr = zeros<std::complex<double>>({1});

int klimit0 = 0;

for (int mm = 0; mm < klimit; mm++)
{
Hx_k = zeros<std::complex<double>>({L});

std::ifstream I_file("I_table.bin", std::ios::binary), J_file("J_tab
val_file("val_table.bin", std::ios::binary);
```

```cpp
if (mm > 0)
{
for (int k = 1; k < mm − 1; k++)
{
auto dum = linalg::vdot(view(A_base, k), x_k);
x_k = x_k − dum*view(A_base, k);
}
}

auto xnorm = sqrt(std::real(linalg::vdot(x_k, x_k)));
x_k = x_k/xnorm;

view(A_base, mm) = x_k;

int i = 0, j = 0;
double val = 0;


while(I_file.read((char*) &i, sizeof(int)))
{
J_file.read((char*) &j, sizeof(int));
val_file.read((char*) &val, sizeof(double));

if(j == 0 && i != j)
{
//strong pulse
val = val*exp(−pow(t*dt − 15, 2)/50.);
if(t*dt > 30){
val = 0;
continue;
}


/// weak pulse
// val = val*exp(−pow((t*dt − 40)/200., 2));
// if(t*dt > 40){
// val = 0 ;
```

```
// continue ;
//}

val = cos (87∗( t∗dt ))∗val ;
}
Hx_k [ i ] += val∗x_k [ j ] ;
Hx_k [ j ] += val∗x_k [ i ] ;


}


a_k = linalg :: vdot ( x_k , Hx_k );
y_tmp = Hx_k − a_k∗x_k ;
rr = linalg :: vdot ( y_tmp , y_tmp ) − pow( b_k , 2);


if ( abs ( rr [0]) < tol )
{
break ;
}


klimit0 ++;
auto b_kp1 = sqrt ( abs ( rr ));
x_kp1 = ( y_tmp − b_k∗x_km1 )/ b_kp1 ;
tridia (mm,mm) = a_k [0];


if (mm < L − 1)
{
tridia (mm, mm + 1) = b_kp1 [0];
tridia (mm + 1, mm) = b_kp1 [0];
}


x_km1 = x_k ;
x_k = x_kp1 ;
b_k = b_kp1 ;
}


if ( klimit0 == 0)
{
```

```
x_k = exp(-j*dt*a_k)*x_k;
}


if(klimit0 != 0)
{
auto H_L = view(tridia, range(0, klimit0), range(0, klimit0));
auto A_base0 = view(A_base, range(0, klimit0));


auto diag_res = linalg::eigh(H_L);
auto H_E = std::get<0>(diag_res);
auto H_states = transpose(std::get<1>(diag_res));


ct = zeros<std::complex<double>>({klimit0});


phases0 = exp(-j*dt*H_E);


for (int i = 0; i < klimit0; i++)
{
for (int lam = 0; lam < klimit0; lam++)
{
view(ct, i) += linalg::vdot(view(A_base, i), linalg::dot(
transpose(A_base0), view(H_states, lam)))*phases0(lam)*
view(H_states, lam)[0];
}
}


x_k = linalg::dot(transpose(A_base0), ct);
}



// if(t == nt - 1)
// {
//    x_k = {0, 0,0,0,0,/**/ sqrt(0.25), sqrt(0.25), 0,0, 0,0, 0,0, 0
```

```
//  sqrt (0.25) , sqrt (0.25) ,  0,0,  0,0,  0,0,  0,0};
//  }

xarray<double> dens = zeros<double>({norb});

xarray<double> dens_uu = zeros<double>({n_xct, n_sct});
xarray<double> dens_ud = zeros<double>({n_xct, n_sct});

int l1 , l2 , l3 ;
int m1, m2, m3;
double prob;

for (int j = 0; j < L; j++)
{
l1 = view(view(states , j), 0)[0];
l2 = view(view(states , j), 0)[1];
l3 = view(view(states , j), 0)[2];
m1 = view(view(states , j), 1)[0];
m2 = view(view(states , j), 1)[1];
m3 = view(view(states , j), 1)[2];

prob = pow(abs(view(x_k , j)), 2)[0];

for (size_t i = 0; i < norb; i++) {
if(l1 == i || l2 == i || l3 == i)
{
view(dens , i) += prob;
}
}

if(l3 >= nat && l3 < nat + n_xct)
{
if(m3 >= nat + n_xct)
{
view(view(dens_ud , l3 - nat), m3 - nat - n_xct) += prob;
}
}
```

```cpp
if (l2 >= nat && l2 < nat + nat + n_xct){
view(view(dens_uu, l2 - nat), l3 - nat - n_xct) += prob;
}
}

if(t == nt - 1)
{
for (size_t i = 0; i < n_xct; i++)
{
for (size_t j = 0; j < n_sct; j++)
{
ent_file_ud << i << " " << j << " " << view(view(dens_ud, i)
, j)[0] << std::endl;
}
}

for (size_t i = 0; i < n_xct; i++)
{
for (size_t j = 0; j < n_sct; j++)
{
ent_file_uu << i << " " << j << " " <<
view(view(dens_uu, i), j)[0] << std::endl;
}
}
}

for (size_t i = 0; i < norb; i++) {
psi0_file << dens[i] << std::endl;
}

std::cout << 100*t/double(nt) <<  std::endl;
}

psi0_file.close();
ent_file_ud.close();
ent_file_uu.close();
```

```cpp
}


int main(){

double dt = 0.02;
double TIME = 140.;
int nat = 3;
int n_sct = 600;
int n_xct = 100;
int norb = nat + n_sct + n_xct;


const std::complex<double> uc(0,1);


std::array<size_t, 3> shape = { 50000000, 2, 3 };
xt::xtensor<int, 3> states1(shape);



xarray<int> gr = {{0, 1, 2},{0, 1, 2}};
view(states1, 0) = gr;
int n = 1;


for (int kx = nat; kx < nat + n_xct; kx++) {
xarray<int> row_k1 = {{1, 2, kx},{0, 1, 2}};
//spin up in kx
view(view(states1, n), 0) = view(row_k1, 0);
view(view(states1, n), 1) = view(row_k1, 1);
n++;
}
//
for (int kx = nat; kx < nat + n_xct; kx++) {
xarray<int> row_k1 = {{0, 1, 2},{1, 2, kx},};
//spin down in kx
view(view(states1, n), 0) = view(row_k1, 0);
view(view(states1, n), 1) = view(row_k1, 1 );
n++;
}
```

```
///////////////// SPIN UP IN X ////////////////////
for (int kx = nat; kx < nat + n_xct; kx++) {
for (int ka = nat + n_xct; ka < nat + n_sct + n_xct; ka++) {
xarray<int> row_ka1 = {{0, 2, kx}, {0, 2, ka}};
view(view(states1, n), 0) = view(row_ka1, 0);
view(view(states1, n), 1) = view(row_ka1, 1);
n++;
}
}


for (int kx = nat; kx < nat + n_xct; kx++) {
for (int ka = nat + n_xct; ka < nat + n_sct + n_xct; ka++) {
xarray<int> row_ka2 = {{0, 2, kx}, {0, 1, ka}};
view(view(states1, n), 0) = view(row_ka2, 0);
view(view(states1, n), 1) = view(row_ka2, 1);
n++;
}
}
for (int kx = nat; kx < nat + n_xct; kx++) {
for (int ka = nat + n_xct; ka < nat + n_sct + n_xct; ka++) {
xarray<int> row_ka3 = {{0, kx, ka}, {0, 1, 2}};
view(view(states1, n), 0) = view(row_ka3, 0);
view(view(states1, n), 1) = view(row_ka3, 1);
n++;
}
}
for (int kx = nat; kx < nat + n_xct; kx++) {
for (int ka = nat + n_xct; ka < nat + n_sct + n_xct; ka++) {
xarray<int> row_ka4 = {{0, 1, kx}, {0, 2, ka}};
view(view(states1, n), 0) = view(row_ka4, 0);
view(view(states1, n), 1) = view(row_ka4, 1);
n++;
}
}
```

```
for ( int kx = nat; kx < nat + n_xct; kx++) {
for ( int ka = nat + n_xct; ka < nat + n_sct + n_xct; ka++) {
xarray <int > row_ka5 = {{0, 1, kx}, {0, 1, ka}};
view ( view ( states1 , n ) , 0 ) = view ( row_ka5 , 0 );
view ( view ( states1 , n ) , 1 ) = view ( row_ka5 , 1 );
n++;
}
}
// // /////////////////////////////////////////////
//
//
// ///////////////SPIN DOWN IN X///////////////////
for ( int kx = nat; kx < nat + n_xct; kx++) {
for ( int ka = nat + n_xct; ka < nat + n_sct + n_xct; ka++) {
xarray <int > row_ka1 = {{0, 2, kx}, {0, 2, ka}};
view ( view ( states1 , n ) , 0 ) = view ( row_ka1 , 1 );
view ( view ( states1 , n ) , 1 ) = view ( row_ka1 , 0 );
n++;
}
}
for ( int kx = nat; kx < nat + n_xct; kx++) {
for ( int ka = nat + n_xct; ka < nat + n_sct + n_xct; ka++) {
xarray <int > row_ka2 = {{0, 2, kx}, {0, 1, ka}};
view ( view ( states1 , n ) , 0 ) = view ( row_ka2 , 1 );
view ( view ( states1 , n ) , 1 ) = view ( row_ka2 , 0 );
n++;
}
}
for ( int kx = nat; kx < nat + n_xct; kx++) {
for ( int ka = nat + n_xct; ka < nat + n_sct + n_xct; ka++) {
xarray <int > row_ka3 = {{0, kx, ka}, {0, 1, 2}};
view ( view ( states1 , n ) , 0 ) = view ( row_ka3 , 1 );
view ( view ( states1 , n ) , 1 ) = view ( row_ka3 , 0 );
n++;
}
}
for ( int kx = nat; kx < nat + n_xct; kx++) {
```

```
for (int ka = nat + n_xct; ka < nat + n_sct + n_xct; ka++) {
xarray<int> row_ka4 = {{0, 1, kx}, {0, 2, ka}};
view(view(states1, n), 0) = view(row_ka4, 1);
view(view(states1, n), 1) = view(row_ka4, 0);
n++;
}
}
for (int kx = nat; kx < nat + n_xct; kx++) {
for (int ka = nat + n_xct; ka < nat + n_sct + n_xct; ka++) {
xarray<int> row_ka5 = {{0, 1, kx}, {0, 1, ka}};
view(view(states1, n), 0) = view(row_ka5, 1);
view(view(states1, n), 1) = view(row_ka5, 0);
n++;
}
}
/////////////////////////////////////////////////


auto states = view(states1, range(0, n));
xarray<std::complex<double>> x0 = zeros<std::complex<double>>({n});
view(x0, 0) = 1; // first seed (ground state)

Lanczos(n, states, x0, dt, 7500, n_xct, n_sct);


}
```